EUROFUSION WPS1-PR(16) 16074

H Hoelbe et al.

A numerical study how a scraper element affects the plasma operation of W7-X

Preprint of Paper to be submitted for publication in
Nuclear Fusion

This work has been carried out within the framework of the EUROfusion Consortium and has received funding from the Euratom research and training programme 2014-2018 under grant agreement No 633053. The views and opinions expressed herein do not necessarily reflect those of the European Commission.

A numerical study how a scraper element affects the plasma operation of W7-X

H. Hölbe, T. Sunn Pedersen, Y. Feng, J. Geiger, S. Bozhenkov
and the W7-X Team

Abstract

For long-pulse operation of Wendelstein 7-X (W-7X) installation of an additional divertor component is being considered to protect the edges of the water-cooled divertor target plates. In this paper, the impact on plasma performance of such a protection element, the scraper element (SE), is analyzed using the state-of-the-art edge transport code EMC3-Eirene, combined with magnetohydrodynamic equilibrium magnetic fields calculated with the code package VMEC-Extender. From this numerical analysis, which is significantly more sophisticated than previous analyses of the SE performance [1] , the following conclusions can be drawn: First, the expected protection capability of the SE is confirmed. Second, the calculated heat load patterns are such that overload of other parts of the plasma-facing components may result from the planned scenario. Third, the SE will cause a significant reduction in the particle exhaust capability of the divertor. These results show that a decision to add SE is not straightforward. It is prudent to test its pros and cons by installation of a SE prototype as early as possible. That possibility is described in a recent paper [2].

1 Introduction

One of the optimization criteria for the stellarator [3] Wendelstein 7-X (W7-X) [4] is the minimization of the bootstrap current (I_{BC}) to a negligible level [5, 6]. This optimization goal can be reached fully for certain magnetic field configurations in W7-X, but there are others with attractive properties that have a still quite small but non-negligible level of I_{BC} [7]. This I_{BC} leads to a toroidal current (I_{tor}) that creates an additional poloidal magnetic field that is not necessarily advantageous for divertor operation: Although the I_{tor} is small (of order 50 kA) compared to e.g. equivalent-size tokamak, the combination of the island divertor topology and the low-shear of W7-X [8, 9], means that the divertor operation is measurably affected [10].

This paper focuses on the divertor operation for one particular operation scenario described in [11]. That scenario has a I_{BC} of 43 kA. The actual net I_{tor}, which affects the edge magnetic topology and therefore divertor operation, is a combination of the I_{BC} and the shielding toroidal currents that are induced in the plasma since it is an excellent electrical conductor. Thus, the I_{tor} in this scenario evolves on a timescale of tens of seconds to minutes - the calculated L/R time is 42 s [11], approaching the I_{BC}.
At the plasma edge, the plasma flows out from the closed magnetic surfaces, into and around the edge island chain. The divertor plates intersect these plasma-filled field lines along toroidally elongated stripes. Following the usual naming conventions, we refer to these elongated lines of plasma heat and particle load on the divertors as *strike lines*. In our scenario, a strike line moves over the edge of the target plate as the I_{tor} evolves [12]. The end of a target plate is capable of less heat removal than the rest of the target plate [13], and in this scenario, the plasma heat load exceeds the engineering capability of some of the target elements in a *transitional phase*, at a point where approximately half (22 kA) of the steady-state I_{tor} (43 kA) is reached. After the I_{tor} has increased further, the heat loads are again compatible

with the engineering limits of the divertor. The overload phase lasts tens of seconds. To lower the heat load of the divertor target plate edge during the transitional phase, an additional divertor target plate was designed, called the SE [14, 15]. A separate SE must be placed in front of each divertor unit (DU) to provide the mentioned protection, i.e. a total of 10 SE would need to be installed.
In this paper the influence of a SE on the plasma behavior is analyzed. First, in Section 2, the impact of the SE on the heat-load distribution on the divertor and other in-vessel components is calculated, to verify its protective capability. This verification is important since the SE has been designed using less sophisticated numerical modeling. In Section 2.1, it is investigated whether other overload situations are present when the The second main topic is the effect of the SE on the scrape-off-layer (SOL), in particular, the effect on the neutral particles which are of importance for the pump efficiency which is again important for the density control (section 3.2). In the last part the question is addressed if the SE will interfere with other planned experiments (section 4).

The analysis is performed with EMC3-Eirene — a rather sophisticated fluid model EMC3 described in [16, 17], combined with an equally sophisticated model for kinetic neutrals (Eirene). This is the first time a study of the SE performance is made using these code packages. Earlier analyses were done using simplified geometries. In addition, it is one of the first calculations at all that combines EMC3-Eirene with an MHD equilibrium magnetic field in the full 3D geometry of W7-X. The MHD calculations are do with the VMEC code [18, 19] including its Extender module [20], allowing for calculation of regions with islands and stochastic field line topologies.

1.1 Simulation parameters

A comprehensive set of plasma parameters and magnetic configurations was used, to obtain an adequate picture of the effects of the SE, given that the

SE, once installed, would be present in all experiments, not just the one experimental scenario for which it was designed: Three different values were used for the density at the separatrix: low: $1.0 \cdot 10^{13}\,\mathrm{cm}^{-3}$, intermediate: $2.0 \cdot 10^{13}\,\mathrm{cm}^{-3}$, high: $3.0 \cdot 10^{13}\,\mathrm{cm}^{-3}$ and three values for the perpendicular transport coefficient low: $0.25\,\mathrm{m}^2/\mathrm{s}$, intermediate: $0.5\,\mathrm{cm}^2/\mathrm{s}$, high: $1.0\,\mathrm{m}^2/\mathrm{s}$. The perpendicular heat diffusivity χ is coupled to the particle diffusivity through $\chi_e = \chi_i = 3 \cdot D$. The heating power of 10 MW is kept constant for all calculations. This is the presently foreseen heating power for steady-state operation (100% ECRH).

2 Protection capabilities

Without the SE, our calculations confirm that the divertor edge is too heavily loaded during the $I_{tor} = 22\,\mathrm{kA}$ transitional phase, and also confirm that the SE reduces the heat load to an acceptable level. The results are shown in Figure 1 and Figure 2. The heat load in the critical region is reduced by a factor of six in the region within 5 cm of the target plate edge, from $\approx 6\,\mathrm{MW/m}^2$ to $\approx 1\,\mathrm{MW/m}^2$. The target element ends have been successfully qualified for up to 3 $\mathrm{MW/m^2}$, so our EMC3-EIRENE simulations confirm the earlier findings [12], that the SE protects the target plate edge during the transitional phase, and that without it, the target element ends would be overloaded.

For the start-up phase (0 kA) and for the final configuration (43 kA), the heat load distributions are, as expected, different. Figure 3a shows the heat load for the 0 kA start-up phase; in this configuration, only a very small amount of flux is going to the divertor edge, and any installed SE would be almost unloaded. Figure 3c shows the heat load for the 43 kA final phase, i.e. when the toroidal currents are fully relaxed. In this phase, no SE is needed for protection; nevertheless, it still intercepts a significant flux of particles and heat that would otherwise arrive near the pumping gap of the divertor. Since

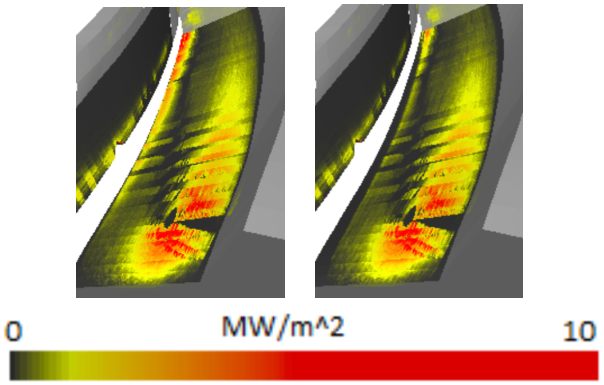

Figure 1: Heat flux at divertor target plates during transitional phase (22 kA. EMC3 result with middle anomalous transport and high density. (a) Without SE. (b) With SE. Calculated with EMC3, for 10 MW heating power.

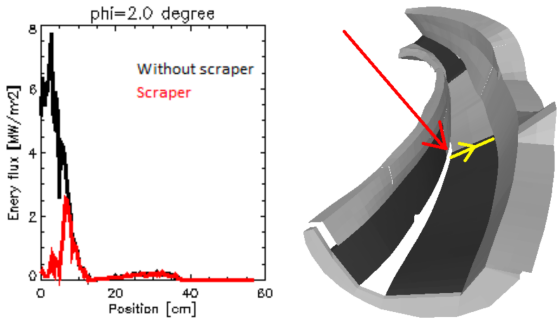

Figure 2: (a) Heat load along a representative line through the critical region (EMC3 result) during the transitional phase (22 kA). EMC3 result with high density and middle anomalous transport. (b) Sketch of measurement location of plot (a).

active pumping at the scraper element is not foreseen, this could compromise the pumping efficiency and hence, density control of W7-X. We will return to this issue in Section 3

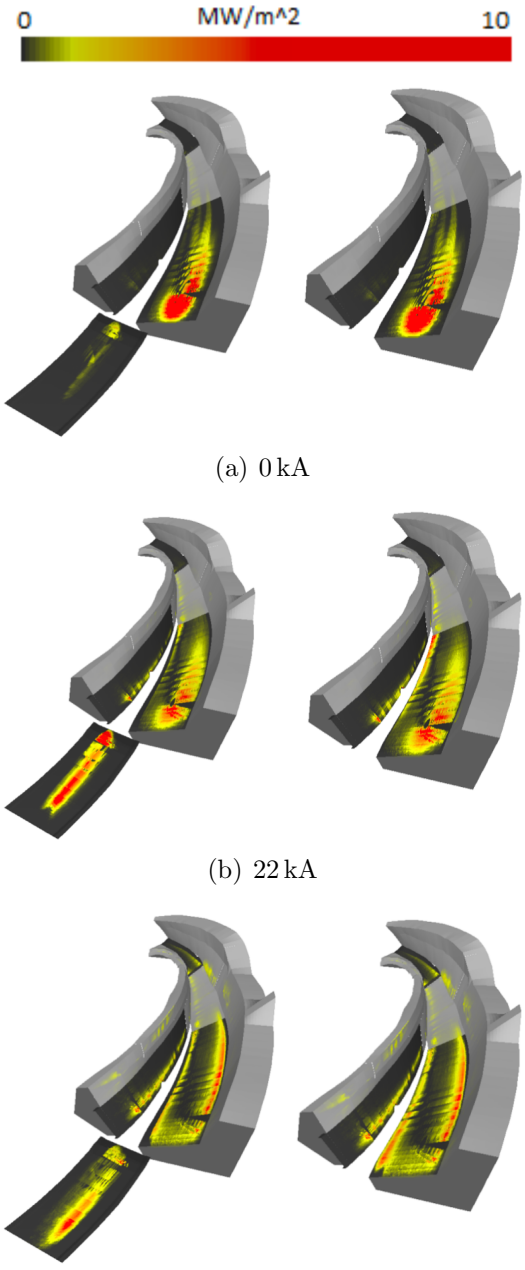

(a) 0 kA

(b) 22 kA

(c) 43 kA

Figure 3: Evolution of toroidal current. EMC3 result with high plasma density and middle anomalous transport. (a) Start-up phase (0 kA). (b) Transitional phase (22 kA). (c) Final configuration (43 kA).

2.1 Protection limits

In order to not interfere with operation for other scenarios, the SE only intersects magnetic field lines that end up near the pumping gap, and does not in general protect other parts of the divertor, nor any other plasma-facing components (PFCs). With the new tools used here, it should be investigated whether other PFCs could be loaded beyond their design limits. We show in the following that, unfortunately, even with the scraper element installed, there are issues with other PFCs exactly for the scenario for which the SE concept was conceived. In figure 4, it is shown that loads onto baffle structures are predicted to exceed their engineering limits, whether or not a SE is installed. Thus, it might be impossible to run this scenario at full power, even with the SE. There are several potential solutions for this problem, such as a re-design of the SE, or repositioning of the baffles, but none of these have been analysed in enough detail that one can clearly say what that would mean. A detailed, self-consistent strategy for this newly discovered issue remains as future work at this point.

2.2 Effect of anomalous transport

EMC3 is capable of simulating perpendicular diffusive transport through a user-defined diffusion coefficient. This can be used to include transport effects that are not explicitly simulated, in particular those due to turbulence. In the predecessor experiment W7-AS, which also had B= 2.5 T on axis, an effective diffusion coefficient of $1\,m^2/s$ at the plasma edge was generally in good agreement with experimental observations. The divertor in W7-X was designed with the assumption of $1\,m^2/s$. Since this prediction has uncertainty, three values of D are used in our simulations, D=0.5 $\mathrm{m/s^2}$ (low), D=1.0 $\mathrm{m/s^2}$ (intermediate), and D= 2 $\mathrm{m/s^2}$ (large).

Figure 5 shows the effect of the strength of the anomalous transport on the strike line patterns. A low transport coefficient leads to narrower strike

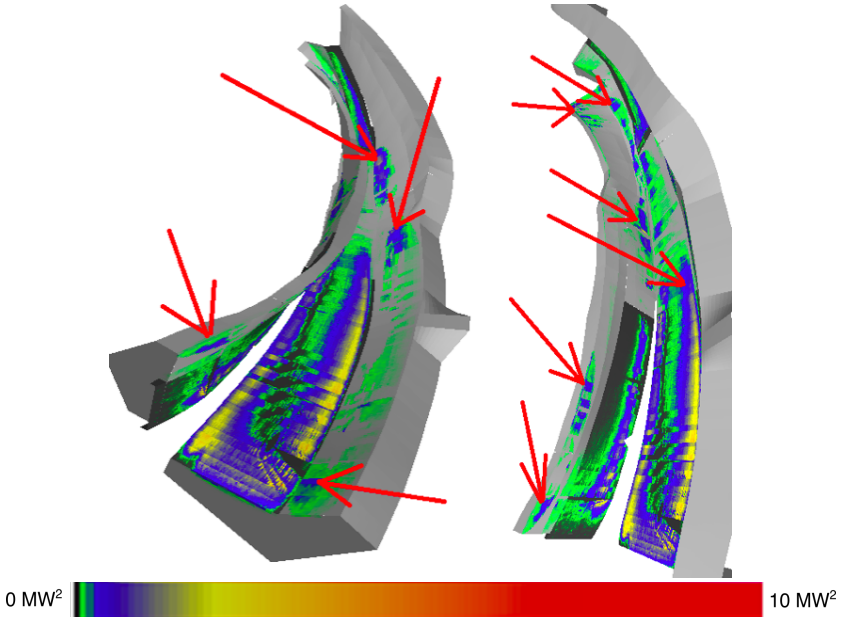

Figure 4: Areas where the baffle plates will get possibly overloaded in the final configuration (43 kA). Calculation with high anomalous transport and high plasma density.

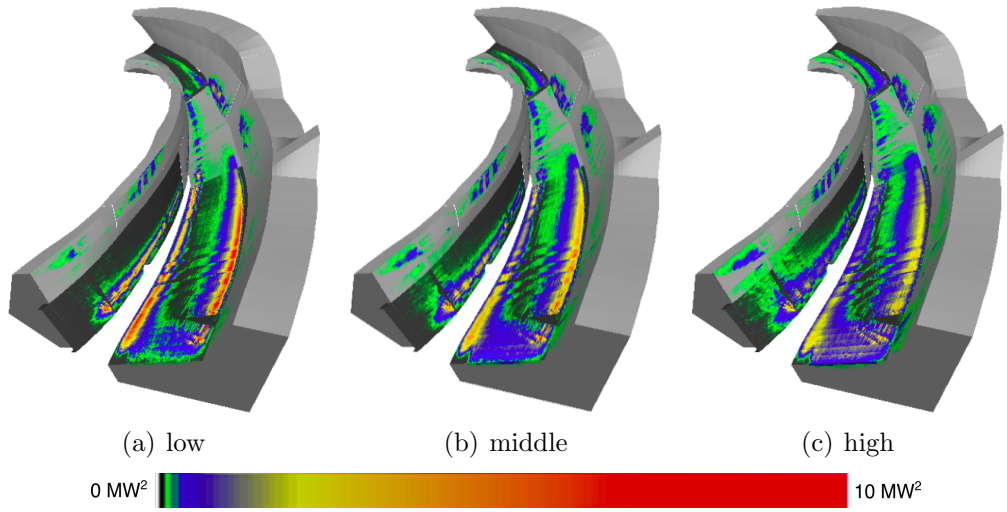

Figure 5: Effect of perpendicular transport on strike lines. Final configuration (43 kA) and high plasma density. (a) Low perpendicular transport. (b) intermediate perpendicular transport. (c) high perpendicular transport.

lines, as one would expect. That concentrates the heat load in a smaller area, which could cause the peak heat flux to exceed engineering limits. A larger transport coefficient would do the opposite, and likely avoid that those strike lines lead to overload - on the other hand, the spreading out of the heat flux could result in heat loads on other PFCs.

2.3 Effect of plasma density

The plasma density at the separatrix may vary from scenario to scenario, and is not necessarily known a priori. Therefore, we also vary this parameter in our simulations. Figure 6 shows the strike line patterns on the divertor for different plasma densities. The plasma density has a large impact on the strike-line width and, therefore, on the local peak heat flux. Given the constant input power, a higher density implies a lower temperature, and therefore, a slower parallel transport because of the high temperature-dependence of the classical heat conductivity. This then allows more perpendicular diffu-

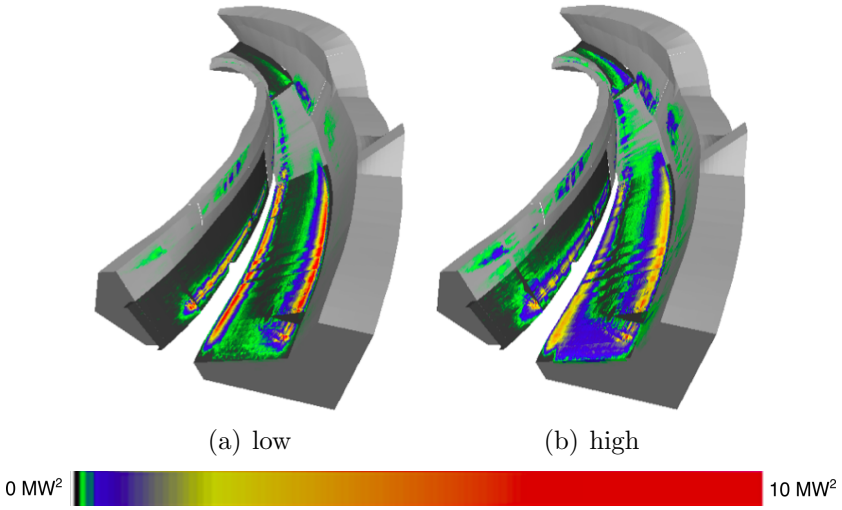

Figure 6: Effect of plasma density on the strike line patterns. For the final configuration (43 kA) and middle anomalous transport coefficient. (a) Low density. (b) high density.

sion to take place, even if one does not change D. Therefore, higher density and higher values of D both lead to wider strike lines. Our numerical calculations confirm this: compare Figures 6 and 5.

2.4 Plasma parameter

The effect of the SE on the bulk plasma parameters, such as density, electron temperature, and ion temperature, are negligible. As an example, we show in Figure 7 that the electron temperature profile is essentially unchanged.

3 Effect on pumping

We now turn our attention to the effects that the SE could have on pumping efficiency. The SE is spatially separated from the divertor pumping gap, under which the divertor pumps will be located. Thus, there is a concern that the SE will act as a poorly pumped limiter, and thereby decrease pumping

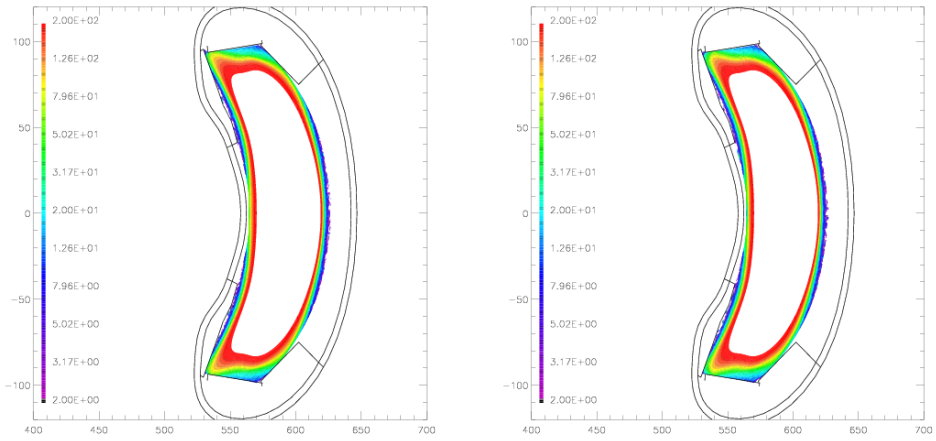

(a) 22 kA without (b) 22 kA scraper

Figure 7: Electron temperature in eV. Results of EMC3-Eirene calculation with high plasma density and middle anomalous transport. (a) 22 kA without a SE (a) 22 kA with a SE

speed.

3.1 Total recycling flux

An ion that hits a plasma-facing component recombines and usually forms a neutral atom, although it could also have a chemical reaction and form a molecule, or be implanted in the PFC. The total rate of neutral particle creation per unit time in the whole device is referred to as the total recycling flux. In Figure 8a, the ion flux calculated by EMC3-Eirene is shown in units of ampere. To convert to hydrogen atoms per second, one divides by the proton charge, $1.602 \cdot 10^{-19}$ C.

The EMC3-Eirene calculations have a number of free parameters that are inputs to the code, i.e. they are not calculated self-consistently. For many of these, a range of values is likely to be experimentally relevant in W7-X divertor operation. We perform scans of several key parameters and attempt to identify trends.

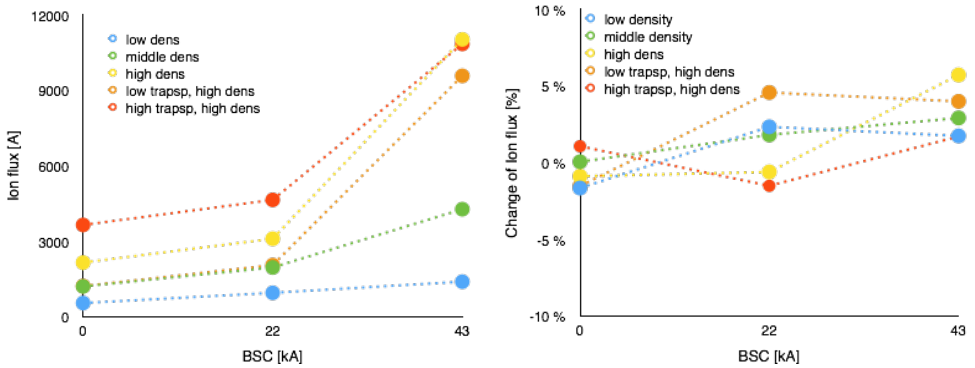

Figure 8: a: Total recycling flux. b: Changes of the total recycling flux due to the SE.

As one might expect, the total recycling flux is higher for higher plasma densities, Figure 8a. In the same Figure, three different values of the perpendicular diffusion coefficient, D at fixed (high) density are also shown. It is seen that increased diffusion also leads to increased recycling flux. This is understandable since the edge plasma density and heating power are prescribed, so that the increased diffusion shortens the particle transport time in the SOL, increasing the recycling flux.

Figure 8b shows the changes of the total recycling flux caused by adding a SE for the aforementioned three points in the discharge evolution (start up, transitional, and end configuration). It is seen that the total recycling flux is essentially unchanged when adding a SE. This is to be expected since the density, heating power, and diffusion coefficients are prescribed. The largest difference seen is 6%, which is on the order of the numerical accuracy.

3.2 Sources of neutrals and pumping efficiency

Figure 9 shows the amount of neutrals created in different configurations and for different simulation parameters.

As expected, there is a correlation between the heat load on the SE and

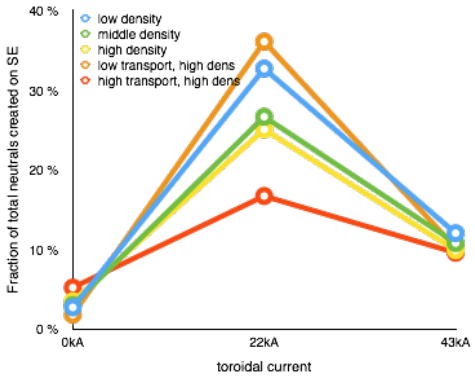

Figure 9: Fraction of total neutral production that originates from the SE.

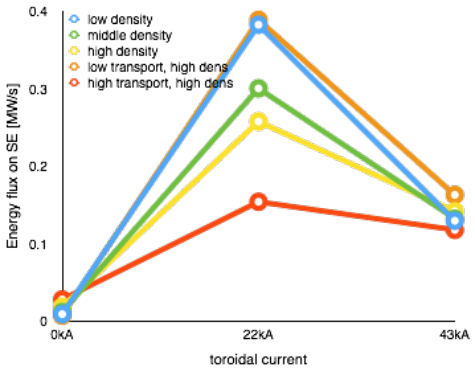

Figure 10: Energy flux on SE.

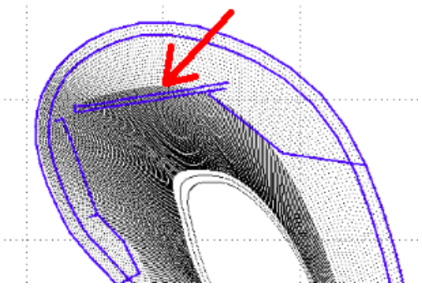

Figure 11: Location of pumping plate in EMC3 pumping simulation. Blue dots: simulation grid resolution.

the neutral particle production on the SE, since the heat is carried by the particles. The exact relation between heat and particle flux onto a material object is a subject of active research [21] but for the purposes of this article it suffices to know that the heat flux Γ_E is related to the particle flux Γ_p through $\Gamma_E == (\gamma_e \cdot Te + \gamma_i \cdot T_i) \cdot \Gamma_p$, with γ_E being a dimensionless constant ([22] page 94), and that EMC3-Eirene calculates heat and particle fluxes explicitly and separately. Thus, it is no surprise that when the scraper element intersects significant heat fluxes, it also intersects significant particle fluxes, and thus, is a location for significant neutral particle production. One should also note that it intersects exactly those particles that would end up at the target edges, adjacent to the pumping gap, so it intersects precisely those that otherwise would have been particularly efficiently pumped away.

During OP2, each of the ten divertor units will be equipped with sub-divertor pumping supplied by cryo-panels and turbo pumps. Because the cryo-panels will have a much larger effective pumping speed, we will, for simplicity, focus exclusively on modeling these. Each of these is simulated as a plate of area 1 m^2, that has a sticking coefficient of 3%. This plate is located at the back of the horizontal divertor plate, as shown in figure 11.

The simulation results for the pumping speed for different parameters with and without the SE are shown in figure 12. In all cases, the installation of an SE reduces the effective pumping speed (particles per second), as one

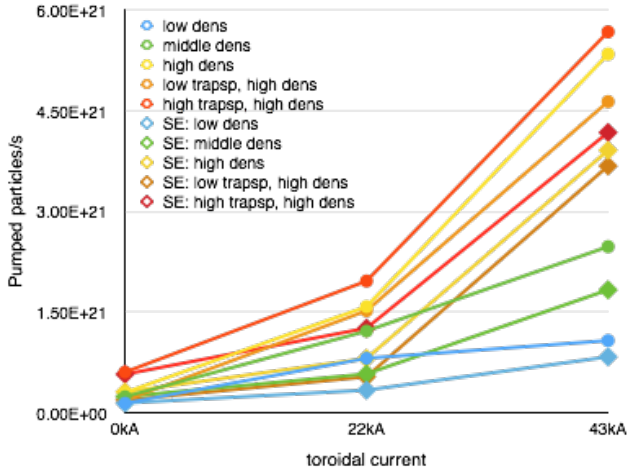

Figure 12: Pumping speed for different plasma parameters and with and without the SE. Absolute numbers here have high uncertainties, but the relative trends should still hold.

would expect from the considerations mentioned earlier. Since the total recycling flux is essentially unperturbed (see subsection 3.1), one concludes that the scraper-element reduces the exhaust efficiency of the divertor accordingly.

The relative pumping speed reduction caused by the SE is shown in figure 13. On average, the pumping is reduced by 52 % in the 22 kA case and by 25 % for the 43 kA case. It is clear that the reduction in pumping for the 22 kA case, is a price that must be paid, if one is to protect the divertor gap in this way. It is also clear that any other strategy that reduces the heat load onto the edge of the fingers, would also cause some reduction in pumping efficiency. However, it was not clear a priori, and is potentially a concern for steady-state density control, that also for the steady-state situation, at 43 kA, there is a significant reduction in the exhaust capability, although the protective features of the scraper element are not needed.

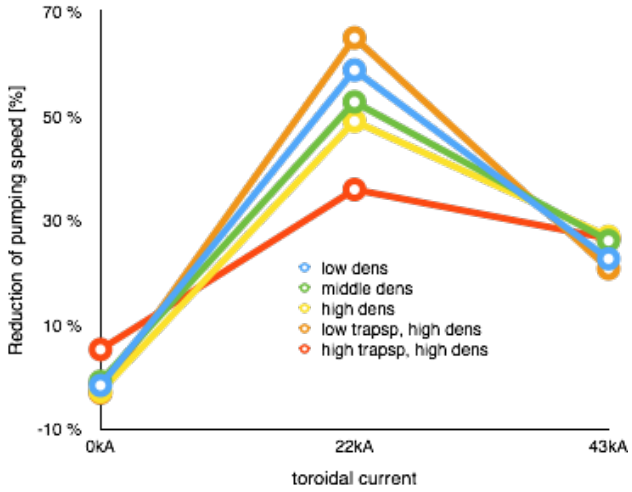

Figure 13: Pumping speed reduction caused by installation of SE

3.3 Consequences of the reduced pumping efficiency

In the following discussion, we focus on analyzing the effects of the reduced pumping caused by the scraper element in the final (43 kA) configuration, since it is the one that is expected to persist for many minutes.

The contribution of the different divertor parts to the neutral production for this configuration is shown in figure 14a; figure 14b shows only the changes caused by the SE. Most of the neutrals are produced at the horizontal divertor plate (hdiv). Only the neutral production at the lower part of this target plate (hdiv bottom) is reduced by the SE. The same amount of neutrals is instead created at the SE. The value is around 10 %, and these 10 % reduce the pumping speed by about 30%.

A look into the details is needed to understand how these small changes can lead to such a big pumping reduction. Figure 15 shows the probability for a neutral particle created at different locations to reach the pump. When looking at the horizontal divertor target plate (hdiv), a neutral particle which is created on the half near the pumping gap has a six times higher probability as an neutral created at the upper part of the hdiv plate to reach the pump.

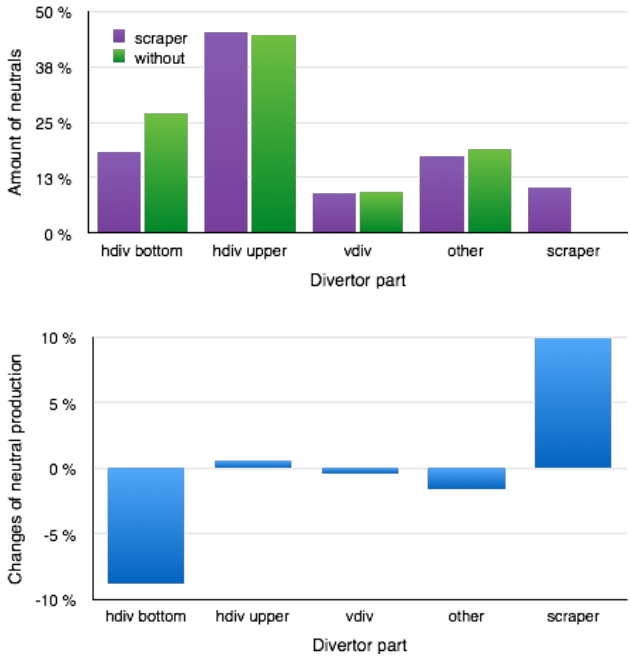

Figure 14: (a) Contribution of different divertor parts to total neutral production. (b) Changes of neutral production caused by the SE. Both figures are for the 43 kA case, intermediate perpendicular transport and intermediate density.

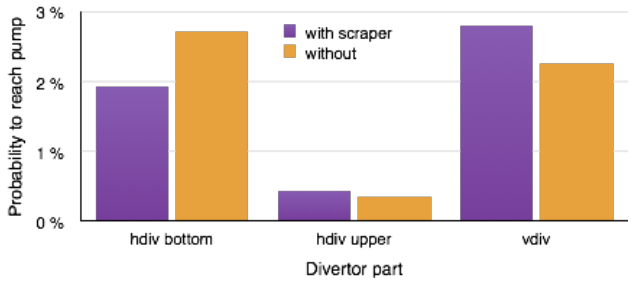

Figure 15: Probability to reach the pump for neutral created at different location. For the 43 kA case, middle anomalous transport and middle density.

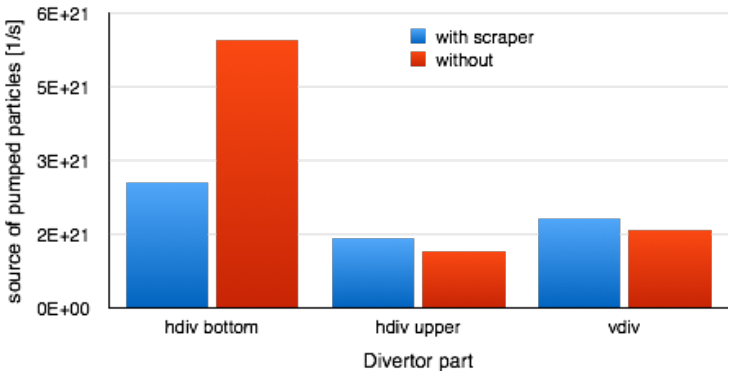

Figure 16: Creation position of pumped particles. For the 43 kA case, middle anomalous transport and middle density.

Neutral particles which are created at the vertical divertor plate (vdiv) also have a high probability to reach the pump, but this area is not shielded by the SE.

Figure 16 shows the pumped particles by their location of creation. With and without the SE, the most important region is the part of the horizontal divertor that is close to the pumping gap. Without SE, the main fraction of the particles reaching the pump originates from the horizontal target near the pumping gap, although only 18 % of the total neutrals are created there. As mentioned, one would expect that particles created near the pumping gap are more efficiently pumped.

4 Other experiments

Given its potential for reducing the pumping efficiency, it is desirable that the SE does not receive significant heat- or particle loads for other planned configurations. In W7-X, the configuration space of most interest is spanned quite well by the so-called *vacuum reference configurations*. A simplified field line diffusion model was used to test this. Although it does not capture many of the dynamics, in particular neutrals, that EMC3-Eirene does, the

Table 1: Percentage of load at the SE for the vacuum reference configurations. Calculation using field line diusion with a perpendicular transport coecient of $1\,m^2/s$ and $T_e = 100\,eV$ (values for T_e=10 eV in parentheses).

Configuration	Fraction of total heat flux on SE [%].
Standard	2.3 (4.6)
Low iota	1.6 (3.5)
High iota	0.0 (0.2)
Low mirror	1.1 (2.6)
High mirror	4.2 (7.7)
Low shear	0.2 (1.8)
Inward shifted	2.3 (7.1)
Outward shifted	0.1 (0.8)
Limiter	0.8 (2.6)

heat load patterns it produces are in rough agreement with those of EMC3-Eirene, and it is a much faster and more easily automated code [23]. The results are shown in Table 1, clearly confirming that the scraper element will not be interacting much with those other configurations. The maximum load is 4.2% for the *high mirror* case.

Nevertheless, the SE will interact with essentially all configurations that load the divertor near the pumping gap. Depending on the experimental scenario this can be desirable (e.g. the 22 kA transitional configuration) or unwanted (e.g. the 43 kA final configuration).

5 Conclusion

In summary, the performed analysis with EMC3-Eirene was able to confirm the protection capability of the SE but also revealed that the SE reduces the pumping capability significantly, even for the final stage of the scraper element reference scenario (SE-RS). Plans for making an early experimental test of the pros and cons of scraper elements are described in detail in a

recent publication [2].

Acknowledgments

This work has been carried out within the framework of the EUROfusion Consortium and has received funding from the Euratom research and training programme 2014-2018 under grant agreement No 633053. The views and opinions expressed herein do not necessarily reflect those of the European Commission.

References

[1] Jeremy D Lore, Tamara Andreeva, Jean Boscary, Sergey Bozhenkov, Joachim Geiger, Jeffrey H Harris, Hauke Hoelbe, Arnold Lumsdaine, Dean McGinnis, Andrew Peacock, et al. Design and analysis of divertor scraper elements for the w7-x stellarator. *Plasma Science, IEEE Transactions on*, 42(3):539–544, 2014.

[2] H. Hölbe, T. S. Pedersen, J. Geiger, S. Bozhenkov, R. König, Y. Feng, and A Lumsdaine. Access to edge scenarios for testing a scraper element in early operation phases of wendelstein 7-x. *Nuclear Fusion*, 56(2), 2016.

[3] Lyman Spitzer Jr. The stellarator concept. *Physics of Fluids (1958-1988)*, 1(4):253–264, 1958.

[4] G Grieger and I Milch. Das fusionsexperiment wendelstein 7-x. *Physikalische Blätter*, 49(11):1001–1005, 1993.

[5] P. Helander and J. Nührenberg. Bootstrap current and neoclassical transport in quasi-isodynamic stellarators. *Plasma Physics and Controlled Fusion*, 2009. 51(5), 055004. ISO 690.

[6] J Nührenberg, W Lotz, P Merkel, C Nührenberg, U Schwenn, E Strumberger, and T Hayashi. Overview on wendelstein 7-x theory. *Fusion Technology*, 27(CONF-941182–), 1995.

[7] *Transport-Simulationen für Wendelstein 7-X*, 2010. Forschungsbericht 2010 - Max-Planck-Institut fr Plasmaphysik, Teilinstitut Greifswald.

[8] P Grigull, K McCormick, J Baldzuhn, R Burhenn, R Brakel, H Ehmler, Y Feng, F Gadelmeier, L Giannone, D Hartmann, et al. First island divertor experiments on the w7-as stellarator. *Plasma physics and controlled fusion*, 43(12A):A175, 2001.

[9] H Renner, J Boscary, H Greuner, H Grote, FW Hoffmann, J Kisslinger, E Strumberger, and B Mendelevitch. Divertor concept for the w7-x stellarator and mode of operation. *Plasma physics and controlled fusion*, 44(6):1005, 2002.

[10] J Geiger, CD Beidler, M Drevlak, H Maassberg, C Nührenberg, Y Suzuki, and Yu Turkin. Effects of net currents on the magnetic configuration of w7-x. *Contributions to Plasma Physics*, 50(8):770–774, 2010.

[11] J Geiger, CD Beidler, M Drevlak, H Maassberg, C Nührenberg, Y Suzuki, and Yu Turkin. Effects of net currents on the magnetic configuration of w7-x. *Contributions to Plasma Physics*, 50(8):770–774, 2010.

[12] J Lore, T Andreeva, J Boscary, JM Canik, J Geiger, Jeffrey H Harris, Arnold Lumsdaine, D McGinnis, A Peacock, and J Tipton. Heat flux and design calculations for the w7-x divertor scraper element. In *Proceedings of the 24th International Atomic Energy Agency Fusion Energy Conference*, 2012.

[13] J Boscary, A Peacock, T Friedrich, H Greuner, B Böswirth, H Tittes, W Schulmeyer, and F Hurd. Design improvement of the target elements

of wendelstein 7-x divertor. *Fusion Engineering and Design*, 87(7):1453–1456, 2012.

[14] Arnold Lumsdaine, Jean Boscary, Eppie Clark, Kivanc Ekici, Jeffrey Harris, Dean McGinnis, Jeremy D Lore, Andrew Peacock, Joseph Tipton, and Jörg Tretter. Modeling and analysis of the w7-x high heat-flux divertor scraper element. *Plasma Science, IEEE Transactions on*, 42(3):545–551, 2014.

[15] Arnold Lumsdaine, Jean Boscary, Joris Fellinger, Jeff Harris, Hauke Hölbe, Ralf König, Jeremy Lore, Dean McGinnis, Hutch Neilson, Peter Titus, et al. Design of the wendelstein 7-x inertially cooled test divertor unit scraper element. *Fusion Engineering and Design*, 2015.

[16] Y Feng, F Sardei, and J Kisslinger. 3d fluid modelling of the edge plasma by means of a monte carlo technique. *Journal of nuclear materials*, 266:812–818, 1999.

[17] Yühe Feng, F Sardei, J Kisslinger, and P Grigull. A 3d monte carlo code for plasma transport in island divertors. *Journal of nuclear materials*, 241:930–934, 1997.

[18] Steven P Hirshman and JC Whitson. Steepest-descent moment method for three-dimensional magnetohydrodynamic equilibria. *Physics of Fluids (1958-1988)*, 26(12):3553–3568, 1983.

[19] SP Hirshman, P Merkel, et al. Three-dimensional free boundary calculations using a spectral green's function method. *Computer Physics Communications*, 43(1):143–155, 1986.

[20] Michael Drevlak, D Monticello, and A Reiman. Pies free boundary stellarator equilibria with improved initial conditions. *Nuclear fusion*, 45(7):731, 2005.

[21] S. Marsen, Eich, T., M. Groth, Jachmich S., B. Sieglin, and JET-EFDA Contributors. Experimental sheath heat transmission factors in diverted plasmas in jet. *Journal of Nuclear Materials*, 2013. 438 (2013): S393-S396.

[22] Peter C Stangeby et al. *The plasma boundary of magnetic fusion devices*, volume 224. Institute of Physics Publishing Bristol, 2000.

[23] SA Bozhenkov, J Geiger, M Grahl, J Kißlinger, A Werner, and RC Wolf. Service oriented architecture for scientific analysis at w7-x. an example of a field line tracer. *Fusion Engineering and Design*, 88(11):2997–3006, 2013.